© 2019. Published by The Company of Biologists Ltd | Development (2019) 146, dev173765. doi:10.1242/dev.173765

RESEARCH ARTICLE

Lin28-mediated temporal promotion of protein synthesis is crucial for neural progenitor cell maintenance and brain development in mice

Stephanie Herrlinger[1,2,*], Qiang Shao[1,*], Mei Yang[1], Qing Chang[1], Yang Liu[3], Xiaohan Pan[4], Hang Yin[3], Li-Wei Xie[4,‡] and Jian-Fu Chen[1,‡]

ABSTRACT

Neural progenitor cells (NPCs) undergo rapid proliferation during neurulation. This rapid growth generates a high demand for mRNA translation in a timing-dependent manner, but its underlying mechanism remains poorly understood. Lin28 is an RNA-binding protein with two paralogs, Lin28a and Lin28b, in mammals. Mice with *Lin28b* deletion exhibit no developmental defects, whereas we have previously reported that *Lin28a* deletion leads to microcephaly. Here, we find that *Lin28a*/*b* double knockout (dKO) mice display neural tube defects (NTDs) coupled with reduced proliferation and precocious differentiation of NPCs. Using ribosomal protein 24 hypomorphic mice (*Rpl24*$^{Bst/+}$) as a genetic tool to dampen global protein synthesis, we found that *Lin28a*$^{-/-}$;*Rpl24*$^{Bst/+}$ compound mutants exhibited NTDs resembling those seen in *Lin28a*/*b* dKO mice. Increased NPC numbers and brain sizes in Lin28a-overexpressing mice were rescued by *Rpl24*$^{Bst/+}$ heterozygosity. Mechanistically, polysome profiling revealed reduced translation of genes involved in the regulation of cell cycle, ribosome biogenesis and translation in dKO mutants. Ribosome biogenesis was reduced in dKO and increased in Lin28a-overexpressing NPCs. Therefore, Lin28-mediated promotion of protein synthesis is essential for NPC maintenance and early brain development.

KEY WORDS: Lin28, Protein synthesis, Ribosome biogenesis, Neural progenitor cell, Neural tube defect

INTRODUCTION

The disruption of the highly complex regulation of neural progenitor cell (NPC) proliferation and growth during neurulation leads to neural tube defects (NTDs) (Greene and Copp, 2014; Wallingford et al., 2013). The proliferation rate is high during early mammalian development. A high level of transcriptional output is required for the fast proliferation of the epiblast in early development (Guzman-Ayala et al., 2015). The global protein synthesis rate and mRNA-specific translation are under precise regulation in distinct cell types during development (Buszczak et al., 2014; Shi and Barna, 2015). The fast proliferation and growth of NPCs in early development generate a high temporally specific demand for protein synthesis, including mRNA translation and ribosome biogenesis. However, neither the impact nor the mechanisms driving protein synthesis have been explored as extensively as transcriptional regulation. How the protein synthesis of rapidly expanding NPCs is temporally regulated in early brain development remains poorly understood.

RNA-binding proteins (RBPs) are capable of mediating coordinated steps of translation. In embryonic stem (ES) cells, hundreds of RBPs have been identified and reported to modulate ES cell self-renewal and pluripotency by regulating post-transcriptional processes, including translational control (Kwon et al., 2013; Ye and Blelloch, 2014). The RBP Hu antigen R (HuR) has been found to play a crucial role in post-transcriptionally regulating neocortical development by dictating the temporal specificity of ribosome composition and functionally related mRNA translation (Kraushar et al., 2014). Loss of function of the RBP FMRP causes Fragile X syndrome, the most common form of inherited intellectual disability. FMRP directly binds to the ribosome and stalls ribosomal translocation on mRNAs encoding proteins involved in synaptic function and autism (Chen et al., 2014; Darnell et al., 2011). Neurulation is a developmental process that occurs after implantation and before neuronal differentiation. RBPs might temporally modulate translation machinery to meet the increased demand for protein synthesis and mRNA translation specificity during rapid NPC expansion in neurulation.

The RBP Lin28 was first discovered to be a crucial heterochronic regulator of cell fate in *Caenorhabditis elegans* larvae (Moss et al., 1997). Lin28 has two homologs, Lin28a and Lin28b, in mammals and contains two types of RNA-binding domains, namely a cold shock domain (CSD) and two CCHC zinc-finger domains. Previous studies have established the importance of the function of Lin28 in a wide range of biological processes and disease conditions, including its roles in ES self-renewal, reprogramming of induced pluripotent stem cells (iPSCs), various cancers and diabetes, among others (Shyh-Chang and Daley, 2013; Thornton and Gregory, 2012). In ES cells, Lin28a associates with ribosomes at the endoplasmic reticulum (ER) and represses the translation of a subset of specific mRNAs destined for the ER (Cho et al., 2012). On the other hand, Lin28a acts as a 'translational enhancer' and promotes translational efficiency in skeletal muscle precursor cells (Polesskaya et al., 2007), suggesting that the mechanism of action of Lin28 is context dependent. The *in vivo* functions of Lin28 in early mammalian embryos are less studied.

We have previously reported that Lin28 is highly enriched in the developing neural tube and exhibits a temporal pattern of expression that decreases as brain development progresses (Balzer et al., 2010; Yang et al., 2015a). Lin28a promotes the proliferative capacity of NPCs in the developing neocortex after neural tube closure (Yang et al., 2015a), leaving its potential functions in neurulation unknown. Here, we report that *Lin28a/b* double knockout (dKO)

[1]Center for Craniofacial and Molecular Biology, University of Southern California, Los Angeles, CA 90033, USA. [2]Biomedical and Health Sciences Institute, Department of Genetics, University of Georgia, Athens, GA 30602, USA. [3]Center for Molecular Medicine, Department of Biochemistry and Molecular Biology, University of Georgia, Athens, GA 30602, USA. [4]State Key Laboratory of Applied Microbiology Southern China, Guangdong Provincial Key Laboratory of Microbial Culture Collection and Application, Guangdong Open Laboratory of Applied Microbiology, Guangdong Institute of Microbiology, Guangzhou, People's Republic of China.
*These authors contributed equally to this work

‡Authors for correspondence (jianfu@usc.edu; xielw@gdim.cn)

Q.S., 0000-0001-5307-8264; J.-F.C., 0000-0002-8869-5913

Received 17 November 2018; Accepted 29 April 2019

Development (2019) 146, dev173765. doi:10.1242/dev.173765

resulted in NTDs in mice. NPC maintenance was impaired, as reflected by reduced proliferation rate and precocious differentiation of NPCs. We employed ribosomal protein hypomorphic mice ($Rpl24^{Bst/+}$) as a genetic tool to dampen global protein synthesis (Barna et al., 2008), and found that *Lin28a* genetically interacts with *Rpl24* in regulating neural tube closure. Increased NPC numbers and brain sizes in *Lin28a*-overexpressing mice were rescued by $Rpl24^{Bst/+}$ heterozygosity. Polysome profiling studies showed that Lin28a/b promotes mRNA translation, and Lin28a localizes to nucleoli and promotes ribosomal biogenesis.

RESULTS

Loss of *Lin28a*/*b* results in NTDs and embryonic lethality

Our previously generated western blot showed that Lin28a and Lin28b are highly expressed during neurulation with sharp downregulation as development proceeds (Fig. S1E;Yang et al., 2015a). To examine its expression at cellular levels, we performed immunohistochemical (IHC) staining and found that Lin28a protein is ubiquitously expressed in NPCs in the E9.5 neuroepithelium (Fig. S1A). By examining E11.5 embryos (Fig. 1A), we found that Lin28a IHC staining displays less signal intensity in ventral midbrain and ventral hindbrain in comparison with forebrain (Fig. S1B). Lin28b is highly expressed in nestin-positive NPCs, which occupy the whole area of E10.5 neuroepithelium (Fig. 1B). Together, these results suggest that *Lin28a/b* are highly expressed in NPCs during neurulation.

We analyzed *Lin28b* KO mice, including E18.5 brain size (Fig. 1D), NPC proliferation and differentiation during neurulation (Fig. 2A-D). We did not detect obvious abnormalities in embryonic morphology or NPC proliferation in $Lin28b^{-/-}$ mutant embryos, and $Lin28b^{-/-}$ mice were born in the expected genotype ratios and survived well, all of which are consistent with published studies (Shinoda et al., 2013). Lin28a and Lin28b are highly conserved with similar amino acid sequences (76%), structures and expression patterns in neuroepithelium. Previously, we found that *Lin28a* single KO mice displayed mild microcephaly, which is exacerbated in the background of $Lin28b^{+/-}$ mice (Yang et al., 2015a), suggesting that they may have overlapping functions in brain development. To thoroughly investigate Lin28a/b function in the developing brain, we crossed $Lin28a^{+/-};Lin28b^{+/-}$ males with females and correlated their genotypes with phenotypes. Among all the different genotypes, $Lin28a^{-/-}$ and $Lin28a^{-/-};Lin28b^{+/-}$ embryos appeared smaller at E12.5 (Fig. 1C), and their brain weights were significantly reduced at E18.5, whereas the other

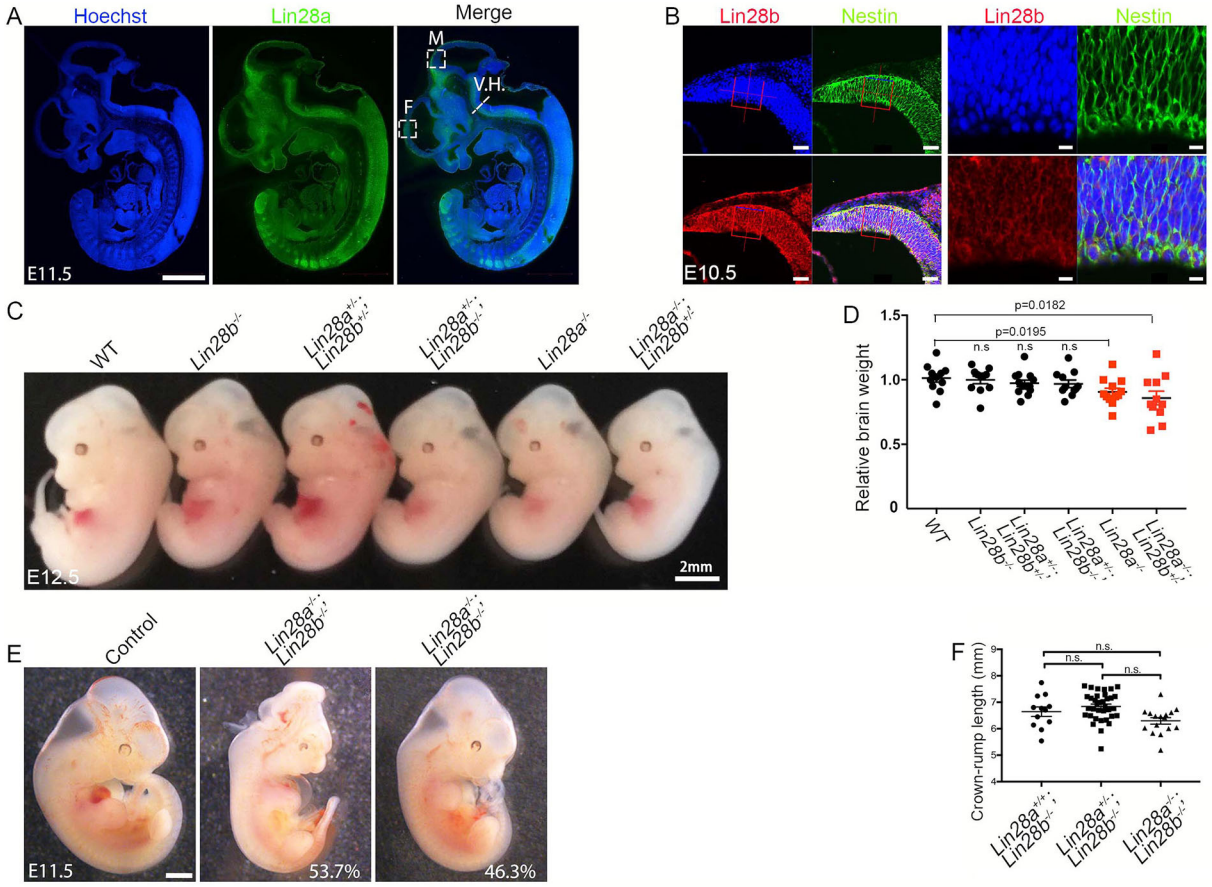

Fig. 1. Loss of *Lin28a*/*b* results in NTDs and embryonic lethality. (A) Confocal microscopy images of E11.5 wild-type embryo sectioned sagittally show Lin28a expression across the entire neural tube. Scale bar: 1 mm. (B) Representative images of neural tube sections stained using antibodies against Lin28b (red) and nestin (green). Right panels are enlargements of boxed areas in left panels. Scale bars: 50 µm (left panels); 10 µm (right panels). (C) Bright-field images of E12.5 embryos. Scale bar: 2 mm. (D) Quantification of relative brain weights from E18.5 brains. Statistical analyses were performed with one-way ANOVA with Bonferroni's post-hoc test (n>10, n.s represents no significant difference detected). (E) Bright-field images of E11.5 control and *Lin28a*/*b* double mutant embryos with (middle panel) or without (right panel) NTDs (controls include $Lin28a^{+/+};Lin28b^{-/-}$, n=102 and $Lin28a^{+/-};Lin28b^{-/-}$, n=207; dKO include $Lin28a^{-/-};Lin28b^{-/-}$, n=41). Scale bar: 1 mm. (F) E11.5 *Lin28a*/*b* dKO embryos do not exhibit a significant decrease in crown/rump ratio compared with littermate controls. Statistical analyses were performed with one-way ANOVA with Bonferroni's post-hoc test based on measurements of $Lin28a^{+/+};Lin28b^{-/-}$ (n=12), $Lin28a^{+/-};Lin28b^{-/-}$ (n=35) and $Lin28a^{-/-};Lin28b^{-/-}$ (n=16) embryos. n.s., not significant. All data are presented as mean±s.e.m.

Development (2019) 146, dev173765. doi:10.1242/dev.173765

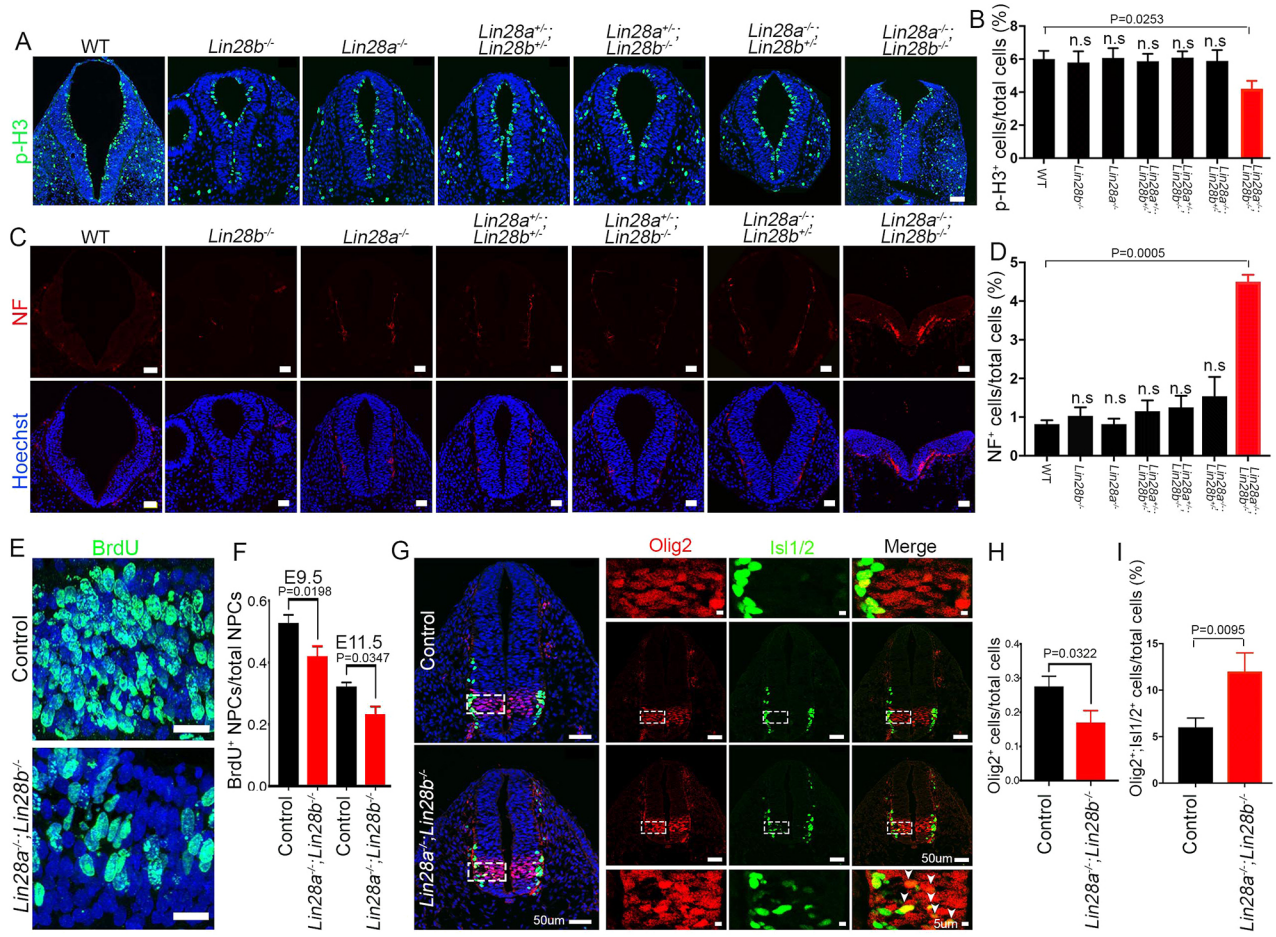

Fig. 2. *Lin28a/b* deletion results in reduced proliferation and precocious differentiation of NPCs. (A) Representative imaging of E9.5 hindbrain sections stained using antibodies against pH3 (green). Hoechst stains nuclei (blue). Scale bar: 50 µm. (B) Quantification of pH3-positive cells out of total cells in E9.5 hindbrain neuroepithelium. (C) Representative imaging of E9.5 hindbrain sections stained using antibodies against neurofilament (NF, red). Hoechst stains nuclei (blue). Scale bars: 50 µm. (D) Quantification of NF-positive cells out of total cells in E9.5 hindbrain neuroepithelium. (E) Representative imaging of E9.5 hindbrain sections stained using antibodies against BrdU after a 0.5 h pulse prior to dissection. Hoechst stains nuclei (blue). Scale bars: 25 µm. (F) Quantification of BrdU-positive NPCs out of total NPCs in E9.5 neuroepithelium or E11.5 ventricular zone (VZ) of cerebral cortex. (G) Representative imaging of E9.5 spinal cord sections stained for Olig2 (red) and Isl1/2 (green). Hoechst stains nuclei (blue). Upper- or lower-most panels are enlargements from boxed areas in the middle panels. White arrowheads indicate Olig2 and Is11/2 double-positive cells in mutant neuroepithelium. Scale bars: 50 µm (left); 5 µm (right). (H,I) Quantification of Olig2 or Olig2 and Isl1/2 double-positive cells out of total cells in boxed areas. All data are presented as mean±s.e.m. using measurements averaged from at least three sections of each mutant embryo (n=3). Statistical analyses were performed with one-way ANOVA with Bonferroni's post-hoc test in B and D or with a non-parametric Mann–Whitney test in F,H,I. n.s., no significant difference detected.

single or compound mutant brain weights were not changed compared with wild type (Fig. 1D). We analyzed embryos recovered from E8.5 to E18.5 and found that fewer *Lin28a*$^{-/-}$;*Lin28b*$^{-/-}$ (referred to here as *Lin28a/b* dKO) mutants were recovered than would be expected from the Mendelian ratio, suggesting their embryonic lethality (Table 1).

Focusing on E8.5-E11.5 embryos, we found that *Lin28a/b* dKO embryos failed to close the neural tube with partial penetrance (Fig. 1E, middle panel, 53.7% penetrance), primarily in the midbrain/hindbrain regions (Fig. S1E). In contrast, *Lin28a*$^{+/-}$;*Lin28b*$^{-/-}$ embryos and mice did not exhibit any apparently abnormal phenotype, whereas *Lin28a*$^{-/-}$ and *Lin28a*$^{-/-}$;*b*$^{+/-}$ displayed mild smaller brain sizes without influence on animal survival. In addition to NTDs, *Lin28a/b* dKO mutants also exhibited other consistent phenotypes, including smaller head size, a straight-backed appearance of the spinal column and shorter tail length (Fig. 1E, middle and far right panel). Despite these defects, crown-rump lengths were not significantly decreased in *Lin28a/b* dKO mutants compared with controls at E11.5 (Fig. 1F). *Lin28a/b* dKO mice were not reliably recovered after E13.5 and could not survive postnatally. Together, these observations suggest that loss of *Lin28a/b* results in NTDs and embryonic lethality in mice.

Table 1. Numbers of embryos recovered alive out of 291 embryos dissected at E8.5-E18.5 stages

Genotype	Observed number (%)	Expected number (%)
Wild type	21 (7.2)	18 (6.25)
Lin28a$^{-/-}$	18 (6.2)	18 (6.25)
Lin28b$^{-/-}$	23 (7.9)	18 (6.25)
Lin28a$^{+/-}$;*Lin28b*$^{+/-}$	75 (25.8)	73 (25)
Lin28a$^{+/-}$;*Lin28b*$^{-/-}$	32 (11.0)	36 (12.5)
Lin28a$^{-/-}$;*Lin28b*$^{+/-}$	40 (13.7)	36 (12.5)
Lin28a$^{-/-}$;*Lin28b*$^{-/-}$	9 (3.1)	18 (6.25)

Parents were *Lin28a*$^{+/-}$;*Lin28b*$^{+/-}$×*Lin28a*$^{+/}$;*Lin28b*$^{+/-}$. Ratios of actual and expected mutant embryos are listed.

Development (2019) 146, dev173765. doi:10.1242/dev.173765

Lin28a/b depletion leads to reduced proliferation and precocious differentiation of NPCs

NPCs proliferate rapidly before and during neural tube closure (Burns and Hassan, 2001). The presence of NTDs and smaller brain sizes suggest loss of NPCs in *Lin28a/b* dKO mice. To examine NPC proliferation, we performed IHC staining using antibodies against phospho-histone3 (pH3), a marker for mitotic cells (Fig. 2A). There is a significant decrease in the percentage of pH3-positive cells out of total cells in *Lin28a/b* dKO hindbrain neuroepithelium at E9.5 (Fig. 2B), a stage when all neuroepithelium cells exhibit NPC features. NPC proliferation is coupled with neural differentiation in the developing embryo (Doe, 2008). We therefore investigated NPC differentiation using neurofilament (NF) to label differentiating neurons in the hindbrain of neural tube. Whereas NF-positive cells appeared in some compound mutants, only *Lin28a/b* dKO mutant embryos exhibited a significant increase in the percentage of NF-positive cells out of total cells in the E9.5 epithelium (Fig. 2D), which is consistent with their NTDs and early embryonic lethality.

We next focused on our analyses of *Lin28a/b* dKO mutants. In addition to E9.5 dKO mutants, E8.5 and E11.5 mutant embryos also exhibited a reduction in the density of pH3-positive NPCs (Fig. S2A,B). This decrease in $pH3^+$ cells could be due to reduced proliferation rate or to increased mitotic progression. To distinguish these two possibilities, we measured the cell proliferation rate with the thymidine analog BrdU (5-bromo-2′-deoxyuridine) after its incorporation into newly synthesized DNA in S phase. BrdU labeling was performed for 30 min to mark NPCs in E9.5 neuroepithelium or in the ventricular zone/subventricular zone (VZ/SVZ) of E11.5 cerebral cortex. There was a significant decrease in the percentage of $BrdU^+$ NPCs out of total NPCs at both stages (Fig. 2E,F). In addition, we found a significant increase in the percentage of TuJ1-positive cells out of total cells in E9.5 *Lin28a/b* dKO mutant neuroepithelium (Fig. S2C,D). Next, we examined motor neuron progenitors and motor neurons, which are labeled by Olig2 and Isl1/2 in the ventral spinal cord (Jessell, 2000). The distribution pattern of the majority of Olig2- and Isl1/2-positive cells is mutually exclusive in wild-type spinal cords (Fig. 2G). In contrast, Olig2 and Isl1/2 double-positive cells were frequently detected in mutants (white arrowheads in Fig. 2G). Statistical analyses revealed a decrease in the percentage of $Olig2^+$ cells and an increase in the percentage of $Olig2^+$;$Isl1/2^+$ cells out of total cells in E9.5 mutant neuroepithelium (Fig. 2H,I). Together, these results suggest that *Lin28a/b* deletion resulted in reduced proliferation and precocious differentiation of NPCs during neurulation.

Programmed cell death occurs in normal embryonic brain development (Kuan et al., 2000); abnormal cell death has been associated with NTDs (Copp, 2005). To determine whether abnormal apoptosis could contribute to NTDs in *Lin28a/b* dKO mice, we performed TUNEL analyses. No significant changes in $TUNEL^+$ cells were detected between dKO mutants and controls at E9.5, a stage when NTDs can be detected in dKO mutants (Fig. S1C,D). Therefore, abnormal apoptosis is likely not an early causative event for NTDs in *Lin28a/b* dKO embryos, despite its potential involvement in embryonic lethality at later stages.

Lin28a and *Rpl24* genetically interact to regulate neural tube closure

To elucidate the functional mechanisms of Lin28, we focused on mRNA translation and used the $Rpl24^{Bst/+}$ ('Belly Spot & Tail') mouse model. $Rpl24^{Bst/+}$ mice contain a hypomorphic allele of ribosomal protein L24 and have been used as a genetic tool for reducing global protein synthesis (Barna et al., 2008; Signer et al., 2014). In ES cells, Lin28a inhibits the translation of a subset of mRNAs destined for the ER (Cho et al., 2012). In contrast, Lin28 functions as a 'translation enhancer' to promote mRNA translation efficiency in skeletal muscle precursor cells (Polesskaya et al., 2007). These studies suggest that Lin28a regulates mRNA translation in a cell type-dependent manner. We employed mouse genetic approaches to investigate the mechanism and functional significance of Lin28-mediated translation regulation. We reasoned that if Lin28a inhibits translation, a global reduction of protein synthesis by $Rpl24^{Bst/+}$ should rescue brain deficits in $Lin28a^{-/-}$ mutant mice. However, if Lin28a promotes translation, further reducing protein synthesis by $Rpl24^{Bst/+}$ in the background of $Lin28a^{-/-}$ should exacerbate its brain defects.

We crossed $Lin28a^{+/-}$;$Rpl24^{Bst/+}$ and $Lin28a^{+/-}$ mice to generate $Lin28a^{-/-}$;$Rpl24^{Bst/+}$ embryos and their littermate controls. We analyzed progeny embryos at various stages, including E11.5, E14.5 and E17.5. $Lin28a^{-/-}$;$Rpl24^{Bst/+}$ embryos exhibited open NTDs at E11.5 (Fig. 3A, far right panel), whereas $Lin28a^{-/-}$ and $Rpl24^{Bst/+}$ embryos did not. Interestingly, this defect closely mimicked the midbrain/hindbrain NTDs in *Lin28a/b* dKO embryos (Fig. 3B). The neural tube failed to close in the midbrain/hindbrain of affected compound mutant embryos, resulting in exencephaly as development progressed to E14.5 (Fig. 3C) and E17.5 (Fig. 3D). NTDs in $Lin28a^{-/-}$;$Rpl24^{Bst/+}$ embryos occurred with 50% penetrance (8/16 $Lin28a^{-/-}$;$Rpl24^{Bst/+}$ embryos), which was similar to the rate of NTDs in *Lin28a/b* dKO mutants (22/41, Table 2). NTDs in $Lin28a^{-/-}$;$Rpl24^{Bst/+}$ embryos occurred at much higher rates than in individual or compound mutant embryos (Table 2). Occasionally, loss of a single copy of *Lin28a* in the background of $Rpl24^{Bst/+}$ also resulted in NTDs (Fig. 3C, second right most, and 3/32 $Lin28a^{+/-}$;$Rpl24^{Bst/+}$ in Table 2). Together, these studies suggest that *Lin28a* and *Rpl24* genetically interact to regulate neural tube closure.

$Rpl24^{Bst/+}$ heterozygosity partially rescues brain size and NPC deficits in *Lin28a*-overexpressing mice

Lin28a deletion and $Rpl24^{Bst/+}$ heterozygosity may converge on the same protein synthesis pathway, leading to more severe NTDs than those seen in individual mutants. Alternatively, they may function through different processes, all of which are required for neural tube closure. To shed light on this issue, we investigated whether dampening protein synthesis is sufficient to rescue NPC deficits in Lin28a-overexpressing brains. Using *Nestin-Cre* mice, we have previously found that NPC-specific overexpression of Lin28a is able to promote Pax6-positive apical NPCs and reduce Tbr2-positive intermediate NPCs, resulting in an abnormally increased ratio of apical NPCs to intermediate NPCs and ultimately enlarged brain size (Yang et al., 2015a). We generated $Lin28OE^{Tg/+}$;*Nestin*-Cre;$Rpl24^{Bst/+}$ compound mice. Embryos were collected at E18.5. While $Lin28OE^{Tg/+}$;*Nestin*-Cre mice exhibited enlarged brain sizes, $Lin28OE^{Tg/+}$;*Nestin*-Cre;$Rpl24^{Bst/+}$ mice displayed brain sizes comparable with those of wild-type controls (Fig. 4A). We performed Hematoxylin and Eosin staining to examine cortical thickness followed by statistical analyses. Cortical thickness was significantly increased in *Lin28a*-overexpressing mice, which is consistent with our previous publication (Yang et al., 2015a). The increased cortical thickness of *Lin28a*-overexpressing brains was rescued by $Rpl24^{Bst/+}$ (Fig. 4B,C), suggesting that protein synthesis is a mediator of the function of Lin28 in promoting brain growth.

To determine whether $Rpl24^{Bst/+}$ can rescue the disrupted balance between apical NPCs and intermediate NPCs in *Lin28a*-overexpressing brains (Yang et al., 2015a), we performed IHC staining for Pax6 to label apical NPCs and for Tbr2 to label

Development (2019) 146, dev173765. doi:10.1242/dev.173765

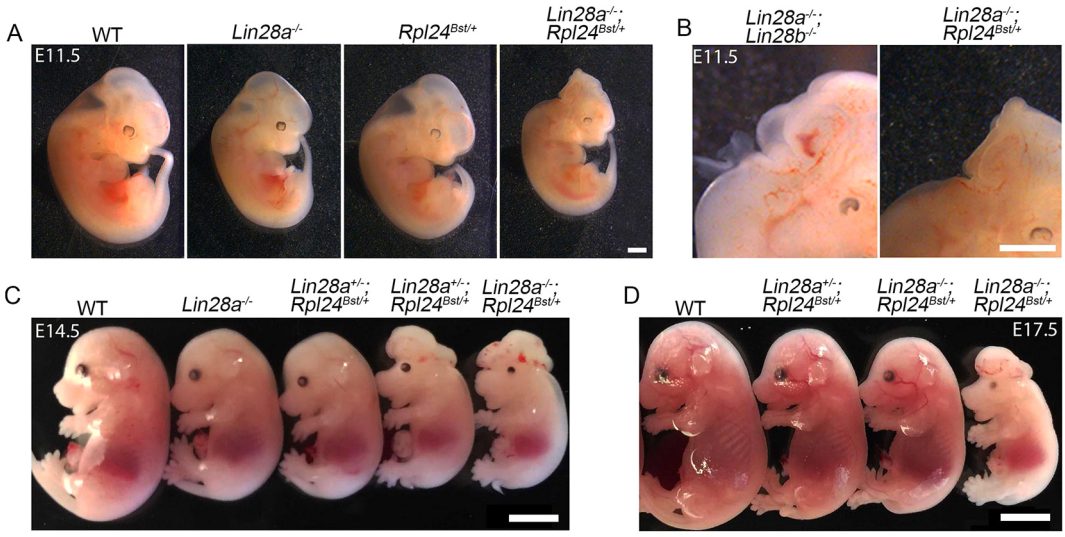

Fig. 3. *Lin28a*$^{-/-}$;*Rpl24*$^{Bst/+}$ mutants mimic *Lin28a/b* double knockout phenotypes in neural tube defects (NTDs) and embryonic lethality. (A) E11.5 *Lin28a*$^{-/-}$; *Rpl24*$^{Bst/+}$ mutant embryos exhibit NTDs compared with littermate controls. Scale bar: 1 mm. (B) *Lin28a*$^{-/-}$; *Rpl24*$^{Bst/+}$ mutant embryos exhibit NTDs in the hindbrain (right panel), similar to *Lin28a/b* dKO embryos (left panel). Scale bar: 1 mm. (C) E14.5 *Lin28a*$^{-/-}$; *Rpl24*$^{Bst/+}$ or *Lin28a*$^{+/-}$; *Rpl24*$^{Bst/+}$ mutant embryos exhibit exencephaly in comparison with littermate controls. Scale bar: 3 mm. (D) *Lin28a*$^{-/-}$; *Rpl24*$^{Bst/+}$ mutant embryos exhibit exencephaly at E17.5. Scale bar: 3 mm.

intermediate NPCs in the VZ/SVZ of the developing brains. *Lin28a* overexpression resulted in an increase in the percentage of Pax6-labeled apical NPCs, which was rescued by *Rpl24*$^{Bst/+}$ heterozygosity (Fig. 4D,E). Similarly, the decreased Tbr2-positive intermediate NPCs in *Lin28a*-overexpressing brains was also rescued by *Rpl24*$^{Bst/+}$. Together, these genetic results suggest that Lin28 functions through, at least in part, promoting protein synthesis as a whole to regulate NPCs and brain development.

Polysome profiling reveals Lin28-mediated translational regulation in individual genes

Having established the roles of Lin28 in promoting global protein synthesis, we attempted to determine its gene-specific translation regulation. We performed sucrose density gradient ultracentrifugation and fractionation using E11.5 wild-type and *Lin28a/b* dKO neuroepithelial tissues (Fig. 5A). E11.5 was selected as the time point for this experiment based on the availability of sufficient materials and on the phenotypic characterization. We pooled equivalent polysome fractions (fractions #11-#25), verified by consistent polysome profiles and post-fractionation RNA concentrations (Fig. 5A). These samples were then used for RNA isolation followed by RNA sequencing (RNA-Seq) and bioinformatic analyses. In parallel, total mRNAs were isolated from corresponding brain tissues followed by RNA-Seq and bioinformatics analyses. Using a log2 fold change cutoff of 1.5, we examined those significantly changed genes (P<0.05) in total mRNA expression levels between wild type and *Lin28a/b* dKO mutants. Expression of only 15 genes was decreased and only 19 was increased at the total mRNA level (Fig. 5B). In contrast, when we examined changes in mRNA levels from polysome fractions, 368 genes were significantly decreased in the mutant polysome fractions, and expression of 187 genes was found to be significantly increased (Fig. 5B). Next, we used a −log10(0.05)=1.3 cutoff to analyze those differentially expressed genes (P<0.05) between wild type and *Lin28a/b* dKO mutants. Individual mRNA expression level changes are depicted using volcano plots, in which blue and red dots represent decreased or increased gene expression levels, respectively, while gray dots indicate unchanged expression. Again, the aberrations in transcript abundance between control and *Lin28a/b* dKO were much more pronounced in polysome mRNAs compared with total mRNAs (Fig. 5C). Therefore, polysome profiling studies suggest that Lin28 regulates mRNA translation.

To determine the pathways in which these dysregulated genes are involved, we performed gene ontology (GO) and Kyoto encyclopedia of genes and genomes (KEGG) analyses. The most significantly decreased biological pathways included GO terms related to ribosome biogenesis and protein synthesis in dKO mutants (Fig. S3A). Meanwhile, increased cellular components in dKO mutants included neurotransmitter complexes and the postsynapse, indicating that genes important for neuronal differentiation were upregulated (Fig. S3B). These results are consistent with the precocious differentiation phenotype observed in *Lin28a/b* dKO mutants. Gene set enrichment analysis (GSEA) suggested that *Lin28a/b* deletion results in downregulation of genes involved in the regulation of cell cycle, ribosome biogenesis, mTORC1 signaling and translation (Fig. 5D-G). To validate our RNA-Seq data, we re-analyzed those top dysregulated genes with published biological significance in brain development. We found that genes related to the cell cycle and protein synthesis were substantially reduced in

Table 2. NTD penetrance for all genotypes generated from crossing of *Lin28a*$^{+/-}$; *Rpl24*$^{Bst/+}$ males with *Lin28a*$^{+/-}$ females, and crossing of *Lin28a*$^{+/-}$; *Lin28b*$^{+/-}$×*Lin28a*$^{+/-}$;*Lin28b*$^{+/-}$

	Wild type	*Lin28a*$^{+/-}$	*Lin28a*$^{-/-}$	*Lin28b*$^{-/-}$	*Lin28a*$^{+/-}$; *Lin28b*$^{+/-}$	*Lin28a*$^{+/-}$; *Lin28b*$^{-/-}$	*Lin28a*$^{-/-}$; *Lin28b*$^{+/-}$	*Lin28a*$^{-/-}$; *Lin28b*$^{-/-}$	*Rpl24*$^{Bts/+}$	*Lin28a*$^{+/-}$; *Rpl24*$^{Bts/+}$	*Lin28a*$^{/-}$; *Rpl24*$^{Bts/+}$
Closed neural tube	22/22	40/41	15/16	23/23	80/81	32/32	38/40	19/41	14/15	29/32	8/16
Neural tube defect	0/22	1/41	1/16	0/23	1/81	0/32	2/40	22/41	1/15	3/32	8/16

Values indicate the number of animals with the defect out of the total number of animals generated.

Development (2019) 146, dev173765. doi:10.1242/dev.173765

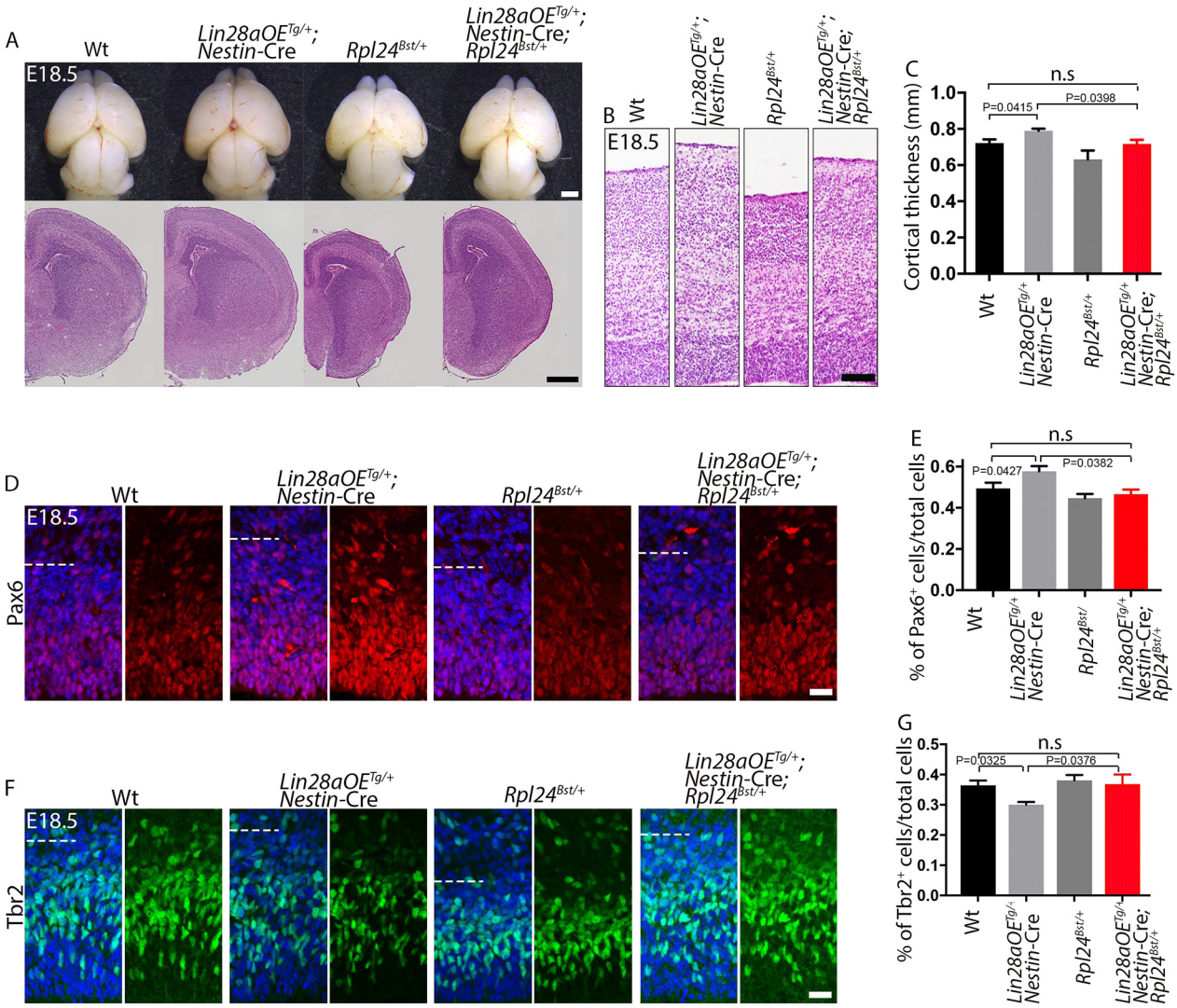

Fig. 4. Abnormally increased brain size and ratio of apical to intermediate NPCs in *Lin28a*-overexpressing mice are rescued by *Rpl24*$^{Bst/+}$ heterozygosity. (A) Dorsal views of E18.5 embryonic brains (top panels) and Hematoxylin and Eosin staining of coronal sections (bottom panels) from wild-type, *Lin28aOE*$^{Tg/+}$*;Nestin*-Cre, *Rpl24*$^{Bst/+}$ and *Lin28OE*$^{Tg/+}$*;Nestin*-Cre;*Rpl24*$^{Bst/+}$ littermates. Scale bar: 1 mm (top panels); 500 µm (bottom panels). (B) Columns of cortices from E18.5 brain sections stained with Hematoxylin and Eosin. Scale bar: 100 µm. (C) Quantification of cortical thickness length from Hematoxylin and Eosin sections represented in B. (D) Confocal micrographs of caudal neocortical coronal sections stained using antibodies against Pax6 (red). Areas underneath the white lines represent ventricular and sub-ventricular zones (VZ/SVZ). Hoechst stains nuclei (blue). Scale bar: 20 µm. (E) Quantification for the ratios of Pax6$^+$ cells/Hoechst$^+$ cells in the E18.5 VZ/SVZ areas from experiments in D. (F) Confocal micrographs of the VZ/SVZ from E18.5 brain sections stained with antibodies against Tbr2 (green). Areas underneath the white lines represent VZ/SVZ. Hoechst stains nuclei (blue). Scale bar: 20 µm. (G) Quantification of the ratios of Tbr2$^+$ cells/Hoechst$^+$ cells in the E18.5 VZ/SVZ areas from experiments in F. All data are mean±s.e.m. using measurements averaged from at least three sections of each mutant embryo (*n*=3). Statistical analyses were performed with one-way ANOVA with Bonferroni's post-hoc test. n.s., no significant difference detected.

polysome-associated mRNA but not in total mRNA measurement (Fig. 5H), suggesting their translational dysregulation. Western blot analysis confirmed downregulation of protein levels of genes involved in the cell cycle (Fig. 5I,J) and ribosome biogenesis (Fig. 5K,L).

Mammalian target of rapamycin complex 1 (mTORC1) is a key regulator of protein synthesis (Laplante and Sabatini, 2012). We have previously reported that Lin28a is associated with mRNAs encoding components of mTORC1 signaling, including Imp1, Akt1, Akt3, Igf2 and Igf1R, and that Lin28a promotes Igf2-mTOR signaling (Yang et al., 2015a). Therefore, we examined mTORC1 activation. S6-kinase (S6K) is phosphorylated by mTORC1, and ribosomal protein S6 (S6) is phosphorylated in turn by S6K, which initiates protein translation (Ferrari et al., 1991; Fingar et al., 2004). Western blot results showed that the expression levels of pS6K and pS6 240/244 were significantly reduced in *Lin28a/b* dKO mutants (Fig. 5M,N). To examine mTORC1 signaling at cellular levels, we performed IHC on hindbrain regions of the neural tube. Both pS6 240/244 and pS6 235/236 signal intensities were reduced in E11.5 dKO mutant neuroepithelium (Fig. S4). Altogether, these data suggest that Lin28a/b enhance mTORC1 signaling and promote translation of genes involved in the cell cycle and ribosome biogenesis.

Lin28a is expressed in nucleoli and promotes ribosome biogenesis in NPCs

RNA-Seq data revealed that genes with decreased expression in *Lin28a/b* dKO mutant polysomes are linked with various pathways related to ribosome biogenesis, including 5.8S ribosome maturation, ribonucleoprotein complex biogenesis and rRNA

Development (2019) 146, dev173765. doi:10.1242/dev.173765

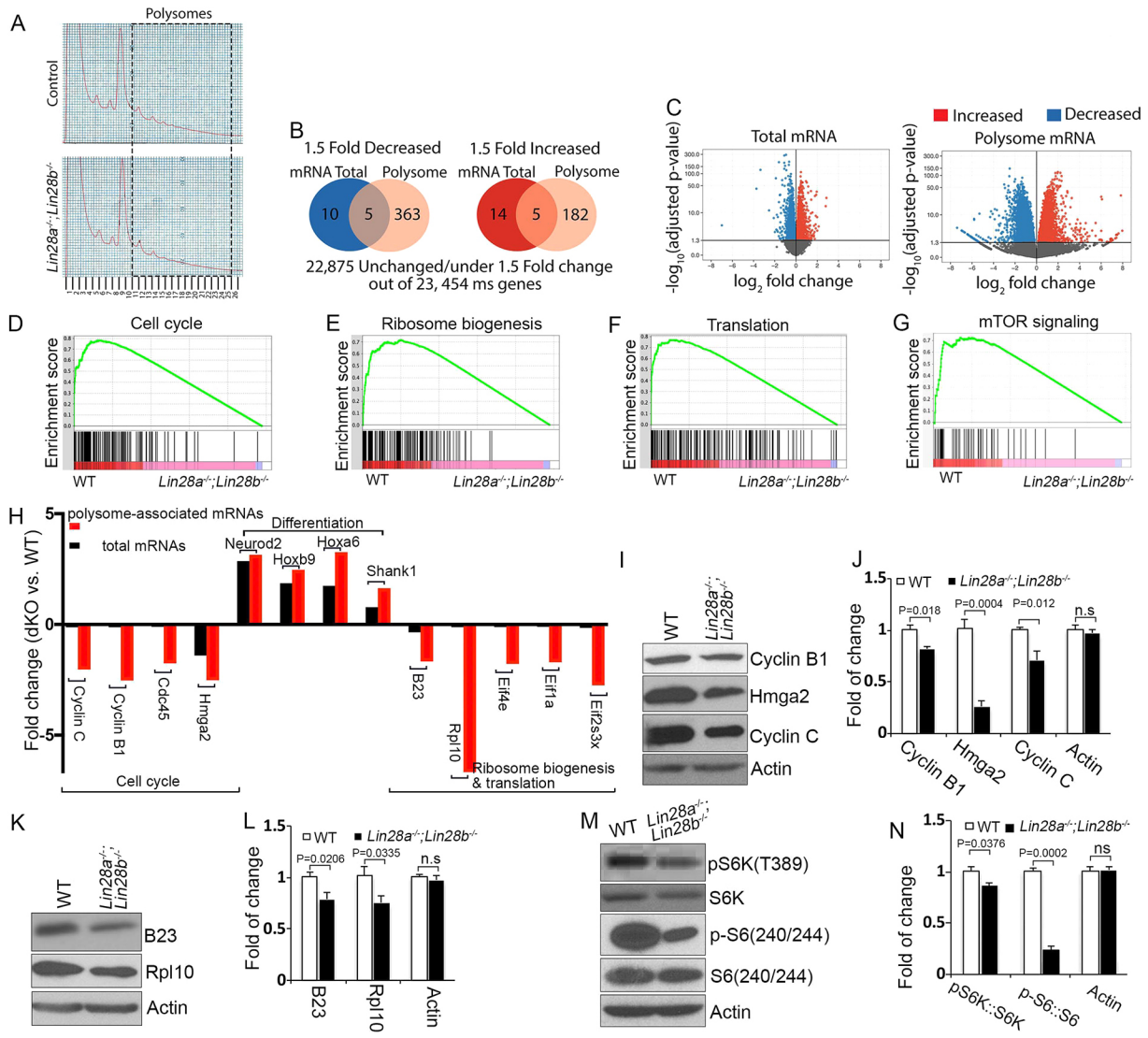

Fig. 5. Lin28-mediated translation regulation revealed by sucrose density gradient fractionation coupled with RNA-seq analysis. (A) Fractions containing polysomes from control and *Lin28a/b* dKO mutant cortical tissues were illustrated through polysome profiling studies, and corresponding fractions (#11-#25) were confirmed by measuring RNA concentration. (B) RNA-seq and bioinformatics analyses of total RNAs or RNAs from polysome fractions derived from E11.5 embryonic brains. Venn diagrams show total and polysome-associated mRNAs that change in abundance in *Lin28a/b* dKO mutants compared with controls. Genes that were expressed differently in wild type and mutants (non-parameter test, $P<0.05$) were analyzed with a Log2(fold change)=1.5 cut off. (C) Volcano plots show gene expression levels relative to controls from a bioinformatic study; blue dots represent transcripts significantly decreased; red dots represent transcripts significantly increased; gray dots represent levels that were not significantly changed. Genes that were expressed differently in wild type and mutants ($P<0.05$) were analyzed with a $-\log10(0.05)=1.3$ cut off. (D-G) Gene set enrichment analysis (GSEA) of polysome-associated mRNAs for gene sets involved in the cell cycle (D), in ribosome biogenesis (E), in translation (F) and in mTORC1 signaling (G). Each line represents a single gene in the gene set. (H) Analysis of RNA-Seq data from total mRNAs and polysome-associated mRNAs reveals translational regulation of genes involved in the cell cycle, neural differentiation, ribosome biogenesis and translation. (I,K,M) Western blot analyses of the expression of proteins as indicated using cortical tissues from E11.5 *Lin28a/b* dKO mutant embryos. (J,L,N) Quantification of western blot data from three independent experiments. The ratios between pS6K versus total S6k or pS6 versus total S6 were calculated (non-parametric Mann–Whitney test; ns, not significant). All data are presented as mean±s.e.m.

processing (Fig. S3A). Western blotting confirmed the downregulation of proteins involved in ribosome biogenesis (Fig. 5K,L). Lin28a localizes to both the nucleolar precursor body (NPB) and mature nucleolus in mouse preimplantation embryos (Vogt et al., 2012). Therefore, we examined the nucleolus, the site of ribosome biogenesis. In addition to the cytoplasm, Lin28a was also highly expressed in the nucleoli, labeled by nucleophosmin (also known as Npm1 or B23), of NPCs during early brain development (Fig. 6A). As development progressed, the nucleolar localization of Lin28a was eliminated at E13.5, whereas its cytoplasmic expression could still be detected (Fig. 6A).

The nucleolus is the site of ribosomal RNA transcription and initial ribosome subunit assembly. Nucleolar size is indicative of ribosome biogenesis and growth (Baker, 2013; Montanaro et al., 2008), and is proportional to the rapidity of cell proliferation in cancer cells (Derenzini et al., 2000). Therefore, we examined nucleolar size in *Lin28a/b* dKO mutant NPCs. Using B23 to label nucleoli, we found that average nucleolar size was significantly decreased in mutant NPCs (Fig. 6B,C), whereas nucleolar numbers appeared normal. In addition to serving as a nucleolar marker, B23 protein has endonuclease activities required for appropriate ribosomal RNA maturation (Savkur and Olson, 1998). Reduced B23 expression is

Development (2019) 146, dev173765. doi:10.1242/dev.173765

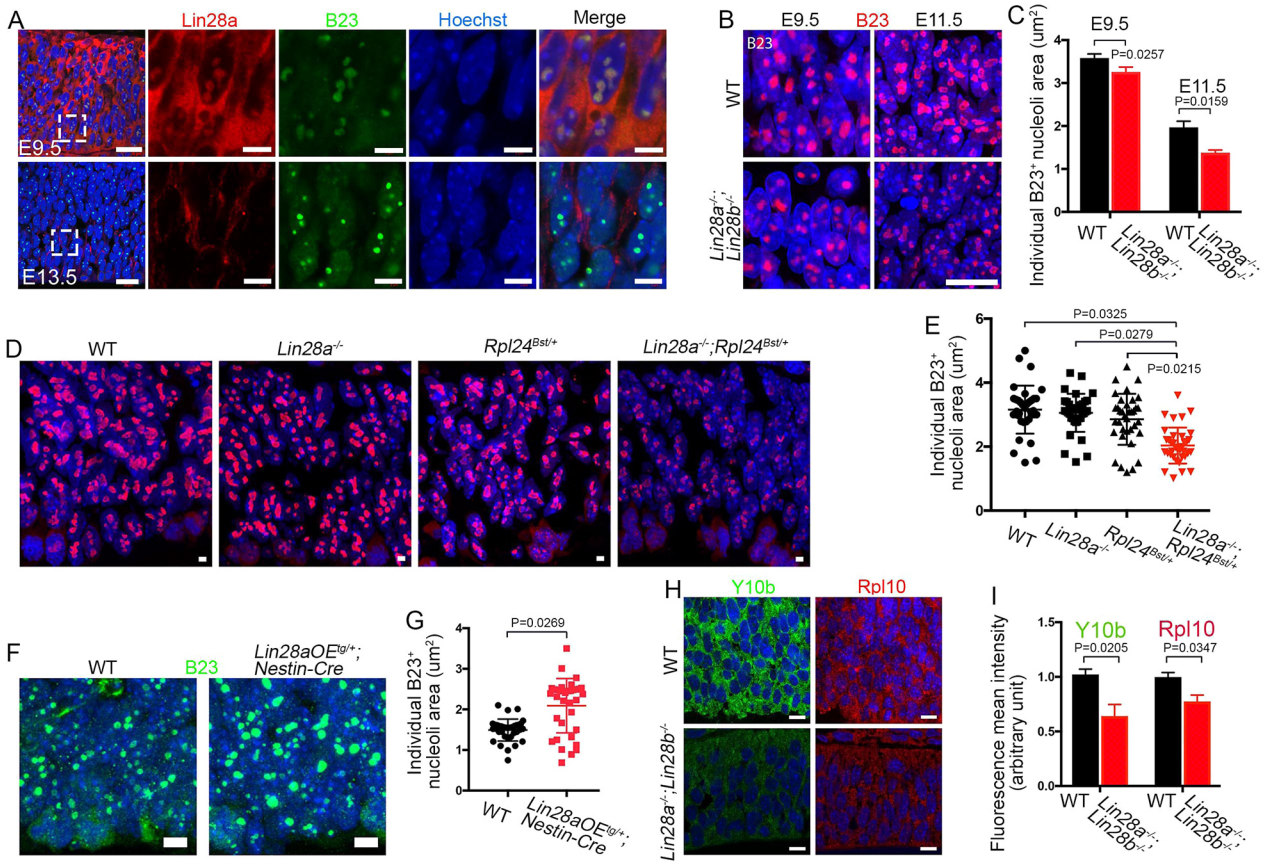

Fig. 6. Ribosome biogenesis is impaired in *Lin28a/b* dKO mutant NPCs. (A) Confocal images of hindbrain sections stained using antibodies against nucleophosmin (B23, green) and Lin28a (red). Hoechst stains nuclei (blue). The boxed areas in the leftmost panels are shown at higher magnification in the images to the right. Scale bars: 20 µm (leftmost panels); 5 µm (right panels). (B) Confocal images of hindbrain sections stained using antibodies against nucleophosmin (B23, red). Hoechst stains nuclei (blue). Scale bar: 10 µm. (C) Quantification of nucleolar mean area. (D) Confocal images of E9.5 hindbrain sections stained with antibodies against B23. Hoechst stains nuclei (blue). Scale bars: 2 µm. (E) Quantification of individual B23-positive nucleolar area from images represented in D (36 individual nucleoli were counted for each experiment). (F) Confocal images of coronal sections of E18.5 cerebral cortex stained with antibodies against B23 (green). Hoechst stains nuclei (blue). Scale bar: 5 µm. (G) Quantification of individual B23-positive nucleolar areas (35 individual nucleoli counted in each experiment). (H) Confocal images of E9.5 hindbrain sections stained with antibodies against Y10b (green) and Rpl10 (red). Hoechst stains nuclei (blue). Scale bars: 10 µm. (I) Quantification of fluorescence mean intensity for Y10b and Rpl10 signals. All data are presented as mean±s.e.m. using measurements averaged from at least three sections of each mutant embryo (n=3). Statistical analyses were performed with one-way ANOVA with Bonferroni's post-hoc test in E or using a non-parametric Mann–Whitney test in C,G,I.

correlated with reduced rRNA transcription (Murano et al., 2008). Western blotting confirmed that the B23 protein level was significantly reduced in *Lin28a/b* dKO neuroepithelial tissues (Fig. 5K,L). Overall, these data indicate that ribosome biogenesis is impaired in mutant NPCs. Next, we examined nucleolus size in *Lin28a*$^{-/-}$, *Rpl24*$^{Bst/+}$ and compound mutant neuroepithelium. *Lin28a*$^{-/-}$; *Rpl24*$^{Bst/+}$ compound mutants exhibited a significant decrease in individual B23-positive nucleolar area compared with *Lin28a*$^{-/-}$ and *Rpl24*$^{Bst/+}$ mutants (Fig. 6D,E). These results suggest that Lin28a and Rpl24 may functionally interact to promote protein synthesis. Conversely, we found a substantial increase in nucleolar size in *Lin28a*-overexpressing NPCs (Fig. 6F,G). Therefore, it appears that Lin28a is sufficient to promote nucleolar size enhancement and ribosome biogenesis. Monoclonal anti-rRNA antibody Y10b specifically labels the 28S subunit of rRNA and serves as a marker of mature ribosomal integrity (Garden et al., 1995; Lerner et al., 1981). We observed significantly reduced Y10b immunoreactivity in *Lin28a/b* dKO neuroepithelium (Fig. 6H,I). The expression of ribosomal protein Rpl10, a key protein in assembling the 60S ribosomal subunit (Ferreira-Cerca et al., 2005), was also reduced in dKO mutant neuroepithelium (Figs 6H,I and 5K,L). Together, these results suggest that Lin28 promotes ribosomal biogenesis, which may contribute to its regulation in protein synthesis.

DISCUSSION

This study revealed that Lin28 acts in the cytoplasm and nucleolus to promote mRNA translation, mTORC1 signaling and ribosomal biogenesis, which collectively contribute to its function in promoting protein synthesis. Lin28 is temporally expressed in early development, and our studies suggest that Lin28-mediated temporal promotion of protein synthesis is crucial for NPC maintenance and early brain development.

We found that Lin28 promotes protein synthesis in NPCs and early brain development *in vivo*. The role of Lin28a in translation regulation remains unclear. Lin28a could inhibit the translation of a subset of mRNAs destined for the ER in ES cells (Cho et al., 2012). On the other hand, Lin28a acts as a 'translational enhancer' in muscle precursor cells (Polesskaya et al., 2007). We previously found that Lin28a is linked with mTORC1 signaling and mRNA translation in the developing brain (Yang et al., 2015a). However, these correlation studies could not determine the causative relationship between Lin28 and translation promotion or its

Development (2019) 146, dev173765. doi:10.1242/dev.173765

functional significance, which thus constitutes the main focus of the present work. Our previous studies showed that Lin28a depletion alone causes mild microcephaly without an impact on animal survival (Yang et al., 2015a). Here, we show that further dampening global protein synthesis by *Rpl24*$^{Bst/+}$ in the background of *Lin28a*$^{-/-}$ leads to NTDs and embryonic lethality, which resemble the phenotypes of *Lin28a/b* dKO mice. This could be explained by *Lin28a*$^{-/-}$ and *Rpl24*$^{Bst/+}$ converging on protein synthesis disruption leading to NTDs, or they may function in different processes required for neural tube closure. However, the fact that *Rpl24*$^{Bst/+}$ heterozygosity partially rescues brain size and NPC deficits in *Lin28a*-overexpressing mice suggests that Lin28 promotes protein synthesis and has a similar function to that of Rpl24. In addition, our polysome profiling studies further support the notion that Lin28 promotes mRNA translation of specific genes involved in the cell cycle, ribosome biogenesis and translation. mTORC1 signaling is a key regulator of protein synthesis (Laplante and Sabatini, 2012). We have previously found that Lin28a associates with multiple mRNAs encoding components of the Igf2-mTOR pathway (Yang et al., 2015a). We detected mTORC1 signaling downregulation in mutant embryos at E11.5, but not at E9.5. These results suggest that mTORC1-related protein synthesis disruption may be not the early causative factor for NTDs in *Lin28a/b* dKO mutants, but contributes to later impairment of protein synthesis and brain development.

Lin28-mediated protein synthesis is crucial for NPC maintenance and early brain development. Previous research has not characterized *Lin28a/b* dKO embryonic phenotypes. Although the involvement of Lin28 in translational regulation has been reported in cultured cells (Cho et al., 2012; Shyh-Chang and Daley, 2013), the biological significance of Lin28-mediated translation at organismic levels remains to be identified. We found that *Lin28a/b* dKO mice exhibited reduced proliferation and precocious differentiation of NPCs and NTDs coupled with embryonic lethality. Abnormal brain size and NPC defects in *Lin28a*-overexpressing mice were partially rescued by *Rpl24*$^{Bst/+}$ heterozygosity. These results suggest that Lin28-mediated promotion of protein synthesis is sufficient to promote proliferation, alter NPC cell fate and drive brain growth. RBPs can modulate cell fate and pluripotency in ES cells via regulating mRNA translation (Ye and Blelloch, 2014). Changes in rRNA transcription influence proliferation and cell fate in ovarian germline stem cells (GSCs) (Zhang et al., 2014). Together with these discoveries, our studies suggest that protein synthesis is tightly linked with the proliferation and cell fate of progenitor cells. It is important to investigate whether, at late stages, *Rpl24*$^{Bst/+}$ heterozygosity can rescue macrocephaly in *Lin28a*-overexpressing mice. Unfortunately, NPC-specific overexpression of *Lin28a* led to variable postnatal phenotypes, including reduced body size and postnatal death (Fig. S5). *Rpl24*$^{Bst/+}$ heterozygous mice exhibited a reduced body size coupled with apoptosis and mitotic arrest in the cerebral cortex at later developmental stages. These complications prevented us from further long-term investigation.

Our studies identify ribosome biogenesis as a novel mechanism of action for Lin28 in promoting protein synthesis. First, Lin28a is highly expressed in the nucleoli, where ribosome biogenesis occurs, in NPCs during early development. Second, nucleolar size was significantly reduced in *Lin28a/b* mutant NPCs, and conversely was increased in *Lin28a*-overexpressing NPCs. *Lin28a*$^{-/-}$;*Rpl24*$^{Bst/+}$ mutants exhibited a reduction in individual nucleolar area compared with *Lin28a*$^{-/-}$ and *Rpl24*$^{Bst/+}$ mutants. These data suggest that Lin28a and Rpl24 functionally interact to regulate ribosome biogenesis. Third, ribosomal integrity is impaired in *Lin28a/b* mutant neuroepithelium, as revealed by reduced expression of Y10b and Rpl10. Nucleolar size is indicative of ribosome biogenesis (Baker, 2013; Montanaro et al., 2008), and is proportional to the rapidity of cell proliferation (Derenzini et al., 2000). Nucleolar size reduction correlates with the decreased proliferation in *Lin28a/b* dKO NPCs. Interestingly, *Lin28a*$^{-/-}$ mutants also exhibited NPC proliferation defects, but nucleolar size reduction was observed only in *Lin28a/b* dKO, not in *Lin28a*$^{-/-}$ mutant NPCs. These results suggest that ribosomal biogenesis disruption is not a major early driving force behind the NPC proliferation defect; instead, it may be a contributing factor. Together, these results suggest that Lin28 modulates nucleolar size and ribosome biogenesis, disruption of which may contribute to protein synthesis reduction in *Lin28a/b* dKO neuroepithelium.

MATERIALS AND METHODS

Ethics statement

All animals were used according to animal use protocols granted by the University of Georgia (Approval # A2016 08-010-Y1-A1) and University of Southern California (Approval # 20718) Institutes of Animal Care and Use Committees (IACUC).

Mouse models

Lin28a$^{-/-}$ knockout mice and *Lin28a* transgenic mice were kindly provided by Eric Moss's laboratory (Rowan University, Glassboro, NJ, USA). The *Lin28b*$^{-/-}$ mice were kindly provided by George Daley's laboratory (Harvard Medical School) and have been described in published studies (Shinoda et al., 2013). Hypomorphic allele *Rpl24*$^{Bst/+}$ (C57BLKS-Rpl24Bst/J, stock # 00516) and *Nestin*-Cre mice [B6.Cg-Tg(Nes-cre)1Kln/J, stock # 003771] were purchased from Jackson Laboratories.

Histology and immunohistochemistry of embryonic tissue

These experiments were performed according to published procedures (Shao et al., 2017). Briefly, embryos were dissected at various stages in development, as noted in the text for each individual experiment (E8.5, E9.5, E11.5, E13.5 and E18.5). Dissected embryos at earlier stages (E8.5-E13.5) remained intact and were fixed in 4% paraformaldehyde for 1 h at room temperature, washed three times in 1× PBS and incubated overnight in 25% sucrose. Embryos were transferred to a solution containing half volume of OCT and half 25% sucrose for 45 min prior to freezing. Fixed embryos were sectioned to a thickness of 12 µm using a cryostat. E18.5 embryonic brain tissue was dissected from the body, and followed the above-mentioned fixation steps thereafter. The secondary antibodies used were Alexa 488 and Alexa 555 conjugated to specific IgG types (Invitrogen Molecular Probes). Primary antibodies were used at concentrations indicated in Table S1. All the experiments have been repeated at least three times, and representative images are shown in the individual figures.

BrdU pulse labeling experiments

BrdU labeling was performed as described previously (Shao et al., 2016; Yang et al., 2015b). Briefly, pregnant dams with stage E11.5 embryos were injected intraperitoneally with BrdU at 10 mg/kg body weight 30 min prior to dissection of the embryos. Immediately after dissection, embryos were fixed in 4% PFA for 1 h at room temperature, subsequently washed in 1× PBS three times for 5 min, and incubated overnight in 25% sucrose. The next day, OCT embedded tissues were then sectioned and stained immunohistochemically with antigen retrieval.

Nucleolar size analyses

FIJI was utilized with the analyze particles toolbox. The nucleoli from *z*-stack images taken every 1 µm of 12 µm sections immunolabeled for nucleophosmin (B23) were subjected to area image analysis.

Polysome fractionation and polysome isolation

Fractionation protocol has been adapted and modified from previous work (Kondrashov et al., 2011; Kraushar et al., 2014). Two replicates were

Development (2019) 146, dev173765. doi:10.1242/dev.173765

performed using neural tube tissues from E11.5 or E12.5 embryos with control or *Lin28a*$^{-/-}$;*b*$^{-/-}$ genotypes.

Sucrose gradients

The day before fractionation, two sucrose gradient solutions were prepared (17% and 51% sucrose) in DEPC-treated water [50 mM NaCl, 50 mM Tris-HCl (pH 7.4) and 10 mM $MgCl_2$]. On the day of fractionation, smaller aliquots were allocated for the sucrose gradients, and 20 mM DTT and 100 µg/ml cycloheximide was added to the aliquots. To generate the gradient, 8.5 ml of 51% sucrose solution was added to a Beckman Coulter Polypropylene Tube (331372). Sucrose (2.5 ml of 17%) was added on top of the dense layer while holding the tube nearly parallel to the ground so as to minimally disturb the higher density sucrose layer. The tube was then covered with parafilm and carefully laid on the bench for 1 h at room temperature.

Sample preparation and fractionation

Prior to fractionation experiments at stage E11.5, embryonic brain tissue was dissected and immediately flash frozen using liquid nitrogen and stored at −80°C. The remaining embryonic tissue was used to confirm genotyping. On the day of fractionation, seven samples were pooled together per genotype in 250 µl polysome buffer [20 mM Tris-HCl (pH 7.4), 100 mM NaCl, 10 mM $MgCl_2$, 1 tablet EDTA-free protease inhibitor, 20 mM DTT, 1% Triton-X100, 1 µg/ml heparin and 100 µg/ml cycloheximide] for 30 min with pipetting every 5 min to homogenize the tissue. Lysate was cleared by centrifugation for 20 min at 14,000 ***g*** at 4°C. Supernatant was collected and RNA concentration was measured using NanoDrop 2000 (ThermoFisher). Supernatant (55 µl) was stored separately at −80°C for total RNA reference sample. The remaining supernatant was carefully applied to the sucrose gradients and ultracentrifuged at 270,000 ***g*** for 160 min at 4°C (SW40 rotor). Gradients were then applied to a tube piercer connected to a Foxy Automated Fractionator and Isco UA-6 UV Detector that measures absorbance at 252 nm. Fractions were collected and their RNA concentration measured prior to RNA extraction from sucrose gradients.

Sucrose extraction and RNA isolation

The high concentration of sucrose in the fractions interferes with the phase separation required in standard Trizol extraction of RNA. To address this issue, we used and adapted an existing published protocol for sucrose extraction from gradient fractions (Clancy et al., 2007). In brief, three volumes of 100% ethanol were added to each fraction and mixed immediately, and the lysate was precipitated overnight at −80°C. The following day, the precipitate was spun at 16,000× ***g*** for 20 min (at 4°C) and supernatant was removed. The resulting pellet was dried by spinning and removal of remaining supernatant. Trizol (1 ml) was added to the pellet and vortexed to dissolve the pellet. After waiting for 5 min for nucleoprotein complexes to dissociate, RNA was then isolated using standard Trizol extraction (Life Biotechnologies).

High-throughput sequencing

Genomic DNA and ribosomal RNA were removed with the Turbo DNA-free kit and the RiboMinus Eukaryote Kit (Life Technologies), respectively. The resulting RNA fractions were subjected to strand-specific library preparation using NEBNext Ultra Directional RNA Library Prep Kit for Illumina (New England Biolabs). Sequencing was performed on a Nextseq500 (Illumina).

RNA-seq assembly and gene enrichment analysis

Raw RNA-seq reads in fastq format were passed through FASTQC to verify quality. The low-quality reads were removed with Fastx-toolkit. The high-quality reads were mapped to the mouse genome (GRCm38/mm10) by TopHat (PMID:19289445) at the optional setting of –G mouse_mRNA.gtf and assembled against mRNA annotation by HTSeq. Differential expression analysis was performed between *Lin28a/b* dKO and control groups using the R package DESeq2 (Love et al., 2014). Genes were considered significant if $P<0.05$. This method was applied for the subgroup analysis on the *Lin28a/b* dKO/control (poly) groups and the *Lin28a/b* dKO/control (total) groups. Heatmaps were generated using the R package pheatmap based on read counts of significantly differentially expressed genes. Volcano plots were generated using the R package ggplot2 based on up- and downregulated significantly differentially expressed genes. The list of genes with significant changes was then separated into four groups according to their log2 fold change (>1.5, >1.25, <−1.5, <−1.25). Gene ontology (GO) and Kyoto encyclopedia of genes and genomes (KEGG) analysis were performed by using R package clusterProfiler for the differentially expressed genes (Yu et al., 2012). The *P* values were corrected for multiple comparisons using the Benjamini-Hochberg method.

Western blot analysis

Samples for western blot analyses were prepared from isolated E11.5 neocortex. For individual studies, the densitometry of individual blot signals from three independent western blot experiments were quantified using Image J software. The individual values for each blot signal were normalized to respective controls followed by the statistical analysis among different samples (Student's *t*-test). The antibodies used and their concentrations are described in Table S1.

Quantitation and statistical analysis

Statistics were run in GraphPad PRISM 7.0 software for all ANOVA and non-parametric Mann-Whitney test. Analyses with two dependent variables were performed with two-way ANOVA with Bonferroni post-hoc analyses. Data in all graphs are represented as mean±s.e.m. $*P\leq0.05$; $**P\leq0.01$; $***P\leq0.001$; ns, not significant.

Acknowledgements

We thank Chen laboratory colleagues for stimulating discussions. We are grateful to Dr Eric G. Moss for *Lin28a*$^{-/-}$ knockout mice and *Lin28a* transgenic mice; and to Dr George Daley's laboratory for *Lin28b*$^{-/-}$. We thank Bridget Samuels for critical reading of the manuscript.

Competing interests

The authors declare no competing or financial interests.

Author contributions

Conceptualization: J.-F.C.; Methodology: M.Y., Q.C., Y.L., X.P., H.Y., L.-W.X., J.-F.C.; Software: Q.S.; Validation: M.Y., X.P., L.-W.X., J.-F.C.; Investigation: S.H., Q.S., M.Y., Q.C., L.-W.X., J.-F.C.; Resources: S.H.; Data curation: S.H., Q.S., X.P.; Writing - original draft: S.H., L.-W.X., J.-F.C.; Writing - review & editing: J.-F.C.; Supervision: J.-F.C.; Project administration: J.-F.C.; Funding acquisition: J.-F.C.

Funding

J.-F.C.'s laboratory is supported by funds from the Associate Dean of Research Fund from the Center for Craniofacial Molecular Biology, Herman Ostrow School of Dentistry at the University of Southern California, and by grants R01NS097231 (to J.-F.C.) and R01NS096176 (to J.-F.C.) from the National Institutes of Health. This work was additionally supported by a National Institute of Health Blueprint Diversity Specialized Predoctoral to Postdoctoral Advancement in Neuroscience (D-SPAN) award F99NS105187-01 (to S.H.) and by a Achievement Rewards for College Scientists (ARCS) Global Impact Award (to S.H.), and was in part supported by a National Institutes of Health training grant 2T32GM007103-42 (to S.H.). Deposited in PMC for release after 12 months.

Data availability

RNA-seq data have been deposited in GEO under accession number GSE131536.

Supplementary information

Supplementary information available online at
http://dev.biologists.org/lookup/doi/10.1242/dev.173765.supplemental

References

Baker, N. E. (2013). Developmental regulation of nucleolus size during Drosophila eye differentiation. *PLoS ONE* **8**, e58266. doi:10.1371/journal.pone.0058266

Balzer, E., Heine, C., Jiang, Q., Lee, V. M. and Moss, E. G. (2010). LIN28 alters cell fate succession and acts independently of the let-7 microRNA during neurogliogenesis in vitro. *Development* **137**, 891-900. doi:10.1242/dev.042895

Barna, M., Pusic, A., Zollo, O., Costa, M., Kondrashov, N., Rego, E., Rao, P. H. and Ruggero, D. (2008). Suppression of Myc oncogenic activity by ribosomal protein haploinsufficiency. *Nature* **456**, 971-975. doi:10.1038/nature07449

Burns, J. L. and Hassan, A. B. (2001). Cell survival and proliferation are modified by insulin-like growth factor 2 between days 9 and 10 of mouse gestation. *Development* **128**, 3819-3830.
Buszczak, M., Signer, R. A. J. and Morrison, S. J. (2014). Cellular differences in protein synthesis regulate tissue homeostasis. *Cell* **159**, 242-251. doi:10.1016/j.cell.2014.09.016
Chen, E., Sharma, M. R., Shi, X., Agrawal, R. K. and Joseph, S. (2014). Fragile X mental retardation protein regulates translation by binding directly to the ribosome. *Mol. Cell* **54**, 407-417. doi:10.1016/j.molcel.2014.03.023
Cho, J., Chang, H., Kwon, S. C., Kim, B., Kim, Y., Choe, J., Ha, M., Kim, Y. K. and Kim, V. N. (2012). LIN28A is a suppressor of ER-associated translation in embryonic stem cells. *Cell* **151**, 765-777. doi:10.1016/j.cell.2012.10.019
Clancy, J. L., Nousch, M., Humphreys, D. T., Westman, B. J., Beilharz, T. H. and Preiss, T. (2007). Methods to analyze microRNA-mediated control of mRNA translation. *Meth. Enzymol.* **431**, 83-111. doi:10.1016/S0076-6879(07)31006-9
Copp, A. J. (2005). Neurulation in the cranial region–normal and abnormal. *J. Anat.* **207**, 623-635. doi:10.1111/j.1469-7580.2005.00476.x
Darnell, J. C., Van Driesche, S. J., Zhang, C., Hung, K. Y. S., Mele, A., Fraser, C. E., Stone, E. F., Chen, C., Fak, J. J., Chi, S. W. et al. (2011). FMRP stalls ribosomal translocation on mRNAs linked to synaptic function and autism. *Cell* **146**, 247-261. doi:10.1016/j.cell.2011.06.013
Derenzini, M., Trerè, D., Pession, A., Govoni, M., Sirri, V. and Chieco, P. (2000). Nucleolar size indicates the rapidity of cell proliferation in cancer tissues. *J. Pathol.* **191**, 181-186. doi:10.1002/(SICI)1096-9896(200006)191:2<181::AID-PATH607>3.0.CO;2-V
Doe, C. Q. (2008). Neural stem cells: balancing self-renewal with differentiation. *Development* **135**, 1575-1587. doi:10.1242/dev.014977
Ferrari, S., Bandi, H. R., Hofsteenge, J., Bussian, B. M. and Thomas, G. (1991). Mitogen-activated 70K S6 kinase. Identification of in vitro 40 S ribosomal S6 phosphorylation sites. *J. Biol. Chem.* **266**, 22770-22775.
Ferreira-Cerca, S., Pöll, G., Gleizes, P.-E., Tschochner, H. and Milkereit, P. (2005). Roles of eukaryotic ribosomal proteins in maturation and transport of pre-18S rRNA and ribosome function. *Mol. Cell* **20**, 263-275. doi:10.1016/j.molcel.2005.09.005
Fingar, D. C., Richardson, C. J., Tee, A. R., Cheatham, L., Tsou, C. and Blenis, J. (2004). mTOR controls cell cycle progression through its cell growth effectors S6K1 and 4E-BP1/eukaryotic translation initiation factor 4E. *Mol. Cell. Biol.* **24**, 200-216. doi:10.1128/MCB.24.1.200-216.2004
Garden, G. A., Hartlage-Rübsamen, M., Rubel, E. W. and Bothwell, M. A. (1995). Protein masking of a ribosomal RNA epitope is an early event in afferent deprivation-induced neuronal death. *Mol. Cell. Neurosci.* **6**, 293-310. doi:10.1006/mcne.1995.1023
Greene, N. D. E. and Copp, A. J. (2014). Neural tube defects. *Annu. Rev. Neurosci.* **37**, 221-242. doi:10.1146/annurev-neuro-062012-170354
Guzman-Ayala, M., Sachs, M., Koh, F. M., Onodera, C., Bulut-Karslioglu, A., Lin, C.-J., Wong, P., Nitta, R., Song, J. S. and Ramalho-Santos, M. (2015). Chd1 is essential for the high transcriptional output and rapid growth of the mouse epiblast. *Development* **142**, 118-127. doi:10.1242/dev.114843
Jessell, T. M. (2000). Neuronal specification in the spinal cord: inductive signals and transcriptional codes. *Nat. Rev. Genet.* **1**, 20-29. doi:10.1038/35049541
Kondrashov, N., Pusic, A., Stumpf, C. R., Shimizu, K., Hsieh, A. C., Xue, S., Ishijima, J., Shiroishi, T. and Barna, M. (2011). Ribosome-mediated specificity in Hox mRNA translation and vertebrate tissue patterning. *Cell* **145**, 383-397. doi:10.1016/j.cell.2011.03.028
Kraushar, M. L., Thompson, K., Wijeratne, H. R. S., Viljetic, B., Sakers, K., Marson, J. W., Kontoyiannis, D. L., Buyske, S., Hart, R. P. and Rasin, M.-R. (2014). Temporally defined neocortical translation and polysome assembly are determined by the RNA-binding protein Hu antigen R. *Proc. Natl. Acad. Sci. USA* **111**, E3815-E3824. doi:10.1073/pnas.1408305111
Kuan, C.-Y., Roth, K. A., Flavell, R. A. and Rakic, P. (2000). Mechanisms of programmed cell death in the developing brain. *Trends Neurosci.* **23**, 291-297. doi:10.1016/S0166-2236(00)01581-2
Kwon, S. C., Yi, H., Eichelbaum, K., Föhr, S., Fischer, B., You, K. T., Castello, A., Krijgsveld, J., Hentze, M. W. and Kim, V. N. (2013). The RNA-binding protein repertoire of embryonic stem cells. *Nat. Struct. Mol. Biol.* **20**, 1122-1130. doi:10.1038/nsmb.2638
Laplante, M. and Sabatini, D. M. (2012). mTOR signaling in growth control and disease. *Cell* **149**, 274-293. doi:10.1016/j.cell.2012.03.017
Lerner, E. A., Lerner, M. R., Janeway, C. A. and Steitz, J. A. (1981). Monoclonal antibodies to nucleic acid-containing cellular constituents: probes for molecular biology and autoimmune disease. *Proc. Natl. Acad. Sci. USA* **78**, 2737-2741. doi:10.1073/pnas.78.5.2737
Love, M. I., Huber, W. and Anders, S. (2014). Moderated estimation of fold change and dispersion for RNA-seq data with DESeq2. *Genome Biol.* **15**, 550. doi:10.1186/s13059-014-0550-8
Montanaro, L., Treré, D. and Derenzini, M. (2008). Nucleolus, ribosomes, and cancer. *Am. J. Pathol.* **173**, 301-310. doi:10.2353/ajpath.2008.070752
Moss, E. G., Lee, R. C. and Ambros, V. (1997). The cold shock domain protein LIN-28 controls developmental timing in C. elegans and is regulated by the lin-4 RNA. *Cell* **88**, 637-646. doi:10.1016/S0092-8674(00)81906-6
Murano, K., Okuwaki, M., Hisaoka, M. and Nagata, K. (2008). Transcription regulation of the rRNA gene by a multifunctional nucleolar protein, B23/nucleophosmin, through its histone chaperone activity. *Mol. Cell. Biol.* **28**, 3114-3126. doi:10.1128/MCB.02078-07
Polesskaya, A., Cuvellier, S., Naguibneva, I., Duquet, A., Moss, E. G. and Harel-Bellan, A. (2007). Lin-28 binds IGF-2 mRNA and participates in skeletal myogenesis by increasing translation efficiency. *Genes Dev.* **21**, 1125-1138. doi:10.1101/gad.415007
Savkur, R. S. and Olson, M. O. (1998). Preferential cleavage in pre-ribosomal RNA byprotein B23 endoribonuclease. *Nucleic Acids Res.* **26**, 4508-4515. doi:10.1093/nar/26.19.4508
Shao, Q., Herrlinger, S., Yang, S.-L., Lai, F., Moore, J. M., Brindley, M. A. and Chen, J.-F. (2016). Zika virus infection disrupts neurovascular development and results in postnatal microcephaly with brain damage. *Development* **143**, 4127-4136. doi:10.1242/dev.143768
Shao, Q., Herrlinger, S., Zhu, Y.-N., Yang, M., Goodfellow, F., Stice, S. L., Qi, X.-P., Brindley, M. A. and Chen, J.-F. (2017). The African Zika virus MR-766 is more virulent and causes more severe brain damage than current Asian lineage and dengue virus. *Development* **144**, 4114-4124. doi:10.1242/dev.156752
Shi, Z. and Barna, M. (2015). Translating the genome in time and space: specialized ribosomes, RNA regulons, and RNA-binding proteins. *Annu. Rev. Cell Dev. Biol.* **31**, 31-54. doi:10.1146/annurev-cellbio-100814-125346
Shinoda, G., Shyh-Chang, N., de Soysa, T. Y., Zhu, H., Seligson, M. T., Shah, S. P., Abo-Sido, N., Yabuuchi, A., Hagan, J. P., Gregory, R. I. et al. (2013). Fetal deficiency of Lin28 programs life-long aberrations in growth and glucose metabolism. *Stem Cells* **31**, 1563-1573. doi:10.1002/stem.1423
Shyh-Chang, N. and Daley, G. Q. (2013). Lin28: primal regulator of growth and metabolism in stem cells. *Cell Stem Cell* **12**, 395-406. doi:10.1016/j.stem.2013.03.005
Signer, R. A. J., Magee, J. A., Salic, A. and Morrison, S. J. (2014). Haematopoietic stem cells require a highly regulated protein synthesis rate. *Nature* **509**, 49-54. doi:10.1038/nature13035
Thornton, J. E. and Gregory, R. I. (2012). How does Lin28 let-7 control development and disease? *Trends Cell Biol.*. **22**, 474-482. doi:10.1016/j.tcb.2012.06.001
Vogt, E. J., Meglicki, M., Hartung, K. I., Borsuk, E. and Behr, R. (2012). Importance of the pluripotency factor LIN28 in the mammalian nucleolus during early embryonic development. *Development* **139**, 4514-4523. doi:10.1242/dev.083279
Wallingford, J. B., Niswander, L. A., Shaw, G. M. and Finnell, R. H. (2013). The continuing challenge of understanding, preventing, and treating neural tube defects. *Science* **339**, 1222002-1222002. doi:10.1126/science.1222002
Yang, M., Yang, S.-L., Herrlinger, S., Liang, C., Dzieciatkowska, M., Hansen, K. C., Desai, R., Nagy, A., Niswander, L., Moss, E. G. et al. (2015a). Lin28 promotes the proliferative capacity of neural progenitor cells in brain development. *Development* **142**, 1616-1627. doi:10.1242/dev.120543
Yang, S.-L., Yang, M., Herrlinger, S., Liang, C., Lai, F. and Chen, J.-F. (2015b). MiR-302/367 regulate neural progenitor proliferation, differentiation timing, and survival in neurulation. *Dev. Biol.* **408**, 140-150. doi:10.1016/j.ydbio.2015.09.020
Ye, J. and Blelloch, R. (2014). Regulation of pluripotency by RNA binding proteins. *Cell Stem Cell* **15**, 271-280. doi:10.1016/j.stem.2014.08.010
Yu, G., Wang, L.-G., Han, Y. and He, Q.-Y. (2012). clusterProfiler: an R package for comparing biological themes among gene clusters. *OMICS* **16**, 284-287. doi:10.1089/omi.2011.0118
Zhang, Q., Shalaby, N. A. and Buszczak, M. (2014). Changes in rRNA transcription influence proliferation and cell fate within a stem cell lineage. *Science* **343**, 298-301. doi:10.1126/science.1246384